Article

Structuring of Abstract Working Memory Content by Fronto-parietal Synchrony in Primate Cortex

Highlights

- Working memory of abstract categories is structured by oscillating neuronal synchrony

- A parieto-frontal channel in the beta band encodes the most recent input

- A fronto-parietal channel in the theta band differentiates between memorized items

- Task-relevant and distracting stimuli are separated by a theta phase-dependent code

Authors

Simon Nikolas Jacob, Daniel Hähnke, Andreas Nieder

Correspondence

simon.jacob@tum.de

In Brief

Multiple visual quantities held in working memory can be separated by oscillating neuronal communication in the primate prefrontal and parietal cortex. Jacob et al. demonstrate frequency-specific channels suitable for selective readout and long-range transmission of task-relevant and distracting stimuli.

CellPress

Structuring of Abstract Working Memory Content by Fronto-parietal Synchrony in Primate Cortex

Simon Nikolas Jacob,[1,2,3,*] Daniel Hähnke,[1] and Andreas Nieder[2]

[1]Department of Neurosurgery, Klinikum rechts der Isar der Technischen Universität München, Ismaninger Str. 22, 81675 Munich, Germany
[2]Animal Physiology Unit, Institute of Neurobiology, Eberhard-Karls-Universität Tübingen, Auf der Morgenstelle 28, 72076 Tübingen, Germany
[3]Lead Contact
*Correspondence: simon.jacob@tum.de
https://doi.org/10.1016/j.neuron.2018.07.025

SUMMARY

How is neuronal activity across distant brain regions orchestrated to allow multiple stimuli to be stored together in working memory, yet maintained separate for individual readout and protection from distractors? Using paired recordings in the prefrontal and parietal cortex of monkeys discriminating numbers of items (numerosities), we found that working memory content is structured by frequency-specific oscillatory synchrony. Parieto-frontal signaling in the beta band carried information about the most recent numerical input. Fronto-parietal coupling in the theta band differentiated between multiple memorized numerosities. Task-relevant and distracting stimuli were nested in spiking activity of single prefrontal neurons, but could be separated by reading out spikes at distinct phases of parietal theta oscillations. The strength of phase-locked, cross-regional memory coding predicted task performance. Frequency-specific communication channels in the fronto-parietal network could enable serial bottom-up and parallel top-down information transmission, providing an important mechanism to protect working memory from interference.

INTRODUCTION

The ability to store and manipulate information in working memory is central to intelligence. It allows behavior to be flexible and follow internal plans and goals rather than fixed stimulus-response associations (D'Esposito and Postle, 2015). Working memory is an active, distributed cognitive process. Large groups of neurons in a widespread brain network with the prefrontal and parietal association cortex as key structures encode memorized information (Dotson et al., 2014; Jacob and Nieder, 2014; Jacob et al., 2016; Liebe et al., 2012; Mendoza-Halliday et al., 2014; Rose et al., 2016; Salazar et al., 2012). Neuronal activity across distant brain regions must therefore be tightly controlled (Fries, 2015; Gupta et al., 2016; Womelsdorf et al., 2007) to be able to store multiple stimuli together in working memory, while preserving separation for individual readout. However, the organizing principles that structure the content of working memory are unknown.

In prefrontal cortex (PFC), multiple memorized items are stored concurrently (Siegel et al., 2009; Warden and Miller, 2007). Single PFC neurons show mixed selectivity; that is, they can represent both relevant and distracting sensory information as well as other task variables (e.g., rules and motor responses) at the same time (Jacob and Nieder, 2014; Parthasarathy et al., 2017; Rigotti et al., 2013). From a computational viewpoint, mixed selectivity confers a significant advantage over highly specialized responses regarding the repertoire of input–output functions that can be implemented (Fusi et al., 2016). On a neurophysiological level, the readout mechanisms are not clear. Synchronized activity might render the exchange of information between neuronal populations precise and selective (Fries, 2015; Womelsdorf et al., 2007). Temporally aligned (coherent) presynaptic and postsynaptic discharges are crucial for effective neuronal communication (Gupta et al., 2016), arguing that hardwired anatomical connections are functionally modulated by oscillatory, rhythmic changes in neuronal excitability.

It has been suggested that short-term memories in PFC could be stored in a multiplexed fashion, parsed into small groups of informative and less informative spikes (Siegel et al., 2009). This would allow a receiver neuronal population to synchronize to the sender in order to decode and retrieve selected information. Indeed, oscillatory synchrony between the prefrontal and parietal cortex is a typical finding in working memory tasks and significantly correlated with behavioral performance (Antzoulatos and Miller, 2016; Dotson et al., 2014; Johnson et al., 2017; Salazar et al., 2012). Using simultaneous multi-electrode recordings in the prefrontal and parietal cortex of monkeys performing a visual working memory task with distractors, we now show that long-range, directed, and frequency-specific neuronal synchrony serves to disentangle co-existing memorized information.

RESULTS

Fronto-parietal Oscillatory Dynamics in Working Memory with Distractors

We trained two rhesus monkeys (*Macaca mulatta*) to maintain the number of visual items (numerosity) in a sample display in working memory but to ignore a subsequently presented
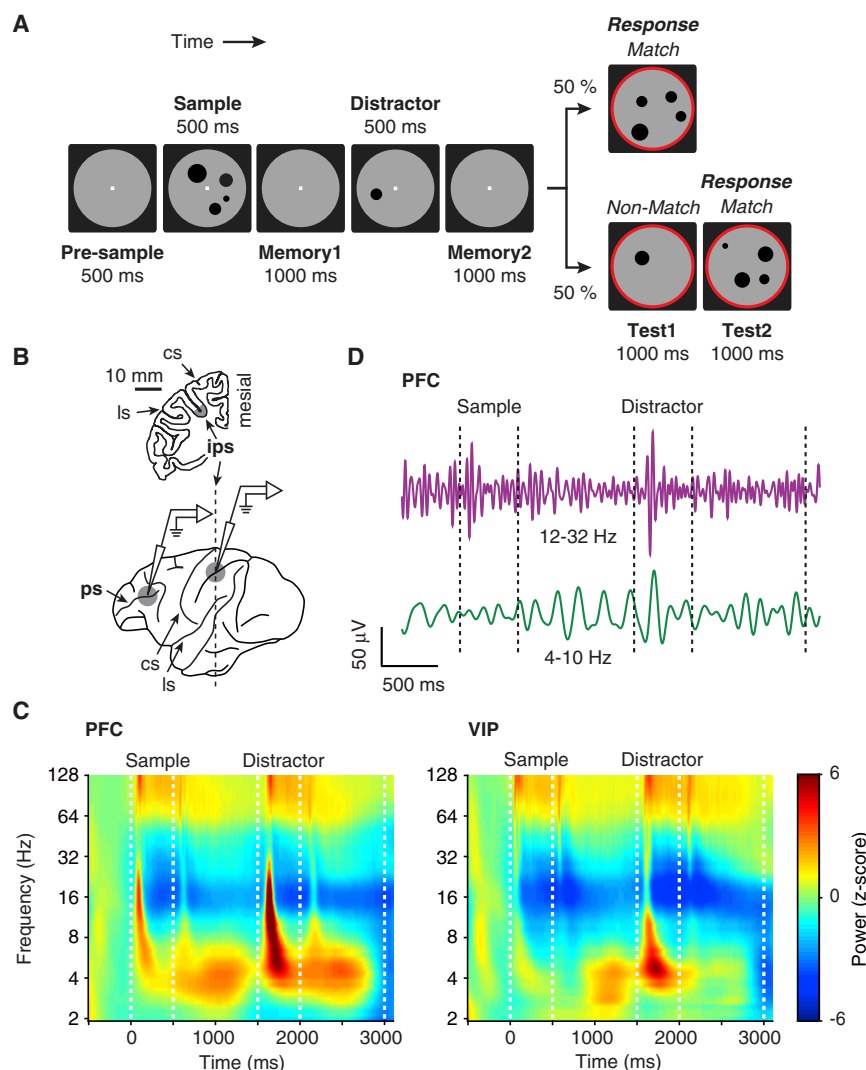
tation of the sample and distractor numerosity elicited a wide-band increase in power in the theta (4–10 Hz), beta (12–32 Hz), and high gamma (>64 Hz) frequency bands. The memory delays were characterized by increased delta (2–4 Hz) and theta activity (particularly in the PFC, Figure 1C, left), whereas beta activity decreased below baseline (particularly in VIP, Figure 1C, right).

Distinct Channels Separating Working Memory Content

To investigate whether the observed neuronal rhythms carried information about the content of working memory, we decoded the sample numerosity from the strength of local oscillatory activity in PFC (Figure 2A) and VIP (Figure 2B) using a Naive Bayes classifier stepped across the trial. We hypothesized that LFP power might scale with the memorized numerical category (i.e., numerosity). Systematic changes of LFP power have been reported, for instance, for working memory load (Jensen and Tesche, 2002; Kornblith et al., 2016; Raghavachari et al., 2001). Memory load, however, would not explain LFP power scaling in our study. We have shown previously that monkeys do not treat each item of the numerosity display as an individual and additional stimulus, but rather assess numerosity at a glance and as a distinct numerical category (Merten and Nieder, 2009; Nieder and Miller, 2004). As a reflection of perceived numerical categories, number neurons are tuned to preferred numerosities (Jacob and Nieder, 2014; Nieder, 2016).

Overall classification accuracy was higher in PFC compared to VIP, but the pattern was similar (Figures 2A and 2B). In the first memory delay, the sample numerosity could be recovered from both lower frequencies (delta and theta bands) and higher frequencies (beta band). By contrast, sample information was lost almost completely from the beta band in the second memory delay and shifted to lower frequencies. Decoding accuracy for the distractor numerosity peaked during distractor presentation

potentially distracting numerosity (Figure 1A). Both animals performed significantly above chance level (monkey R: 72%, p < 10^{-8}, Wilcoxon signed rank test, 47 sessions; monkey W: 71%, p < 10^{-5}, 31 sessions), demonstrating that they were able to separate task-relevant and distracting numerosities in working memory (Jacob and Nieder, 2014). While the animals performed the task, we simultaneously recorded wide-band extracellular neuronal activity, composed of single unit spiking and local field potentials (LFPs), i.e., rhythmic activity across a neuronal population, from the prefrontal cortex (PFC; 616 recording sites) and the ventral intraparietal area (VIP; 614 recording sites) of the posterior parietal cortex (Figure 1B; Figure S1).

LFPs were modulated by different epochs of the task in both brain regions (Figures 1C and 1D) (Antzoulatos and Miller, 2016; Johnson et al., 2017; Liebe et al., 2012; Lundqvist et al., 2016; Pesaran et al., 2002; Siegel et al., 2009). For all analyses involving LFPs, we subtracted the stimulus-locked responses, i.e., the low-frequency "evoked potential," from the raw voltage traces during pre-processing (Siegel et al., 2009). Visual presen-
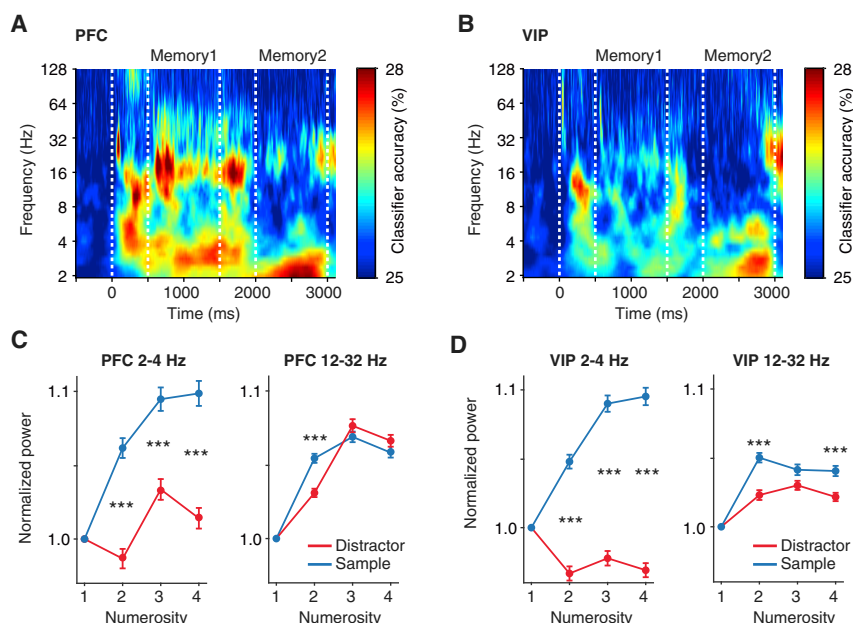
Figure 2. Distinct Frequency Channels Separating Working Memory Content
(A) Naive Bayes decoding accuracy (percent correct) of sample numerosity from LFP power recorded in PFC.
(B) Same analysis as in (A) for VIP.
(C) LFP power in PFC in the second memory delay as a function of sample and distractor (normalized to numerosity 1) in the delta (2–4 Hz; left panel) and beta frequency band (12–32 Hz; right panel).
(D) Same analysis as in (C) for VIP. Error bars indicate SEM across sites. ***p < 0.001 (Wilcoxon signed rank test). See also Figure S2.

were present in the lower-frequency bands (Figure 3C). The reverse, VIP-to-PFC direction was characteristic of the beta band. Thus, compared to baseline, fronto-parietal signaling increased during the memory delays, while parieto-frontal influences were dominant during visual stimulus presentation (Figure 3D). We found the same frequency- and task-specific directed signaling in an analysis of Wiener-Granger causality (Figure S3). Synchrony measures are sensitive to the choice of referencing. We therefore also performed the PLV and PSI analysis with LFP traces re-referenced locally to the average of each recording chamber (Figure S4). The PLV showed even stronger theta connectivity in the memory delays (Figure S4A), supporting our original findings. The control PSI analysis was almost indistinguishable from its counterpart with common-average referencing (Figure S4B).

Third, we measured cross-regional spike-field locking (i.e., alignment of spikes in a "sender" region to specific phases of an LFP oscillation in a "receiver" region), which is indicative of directed synaptic influences (Liebe et al., 2012; Pesaran et al., 2008; Salazar et al., 2012). We tested a total of 4,956 PFC_{unit} – VIP_{LFP} and 3,525 VIP_{unit} – PFC_{LFP} pairs for significant phase locking in the second memory delay (p < 0.05, Rayleigh test for non-uniformity). In agreement with our previous results, fronto-parietal signaling dominated in the lower frequencies, while the parieto-frontal direction was more pronounced in the beta band (locked pairs at 3 Hz: 1,745 versus 973, 20 Hz: 990 versus 1,149, p < 10^{-35}, Fisher's exact test; Figure 3E). An analysis of cross-regional spike-field phase locking (PLV) with all neurons recorded in the second memory delay (PFC: n = 444, VIP: n = 359) supported these findings (Figure 3F).

but was weak in the second memory delay (Figure S2). Low-frequency LFP power in both regions showed a strong preference for the sample over the distractor numerosity and increased non-linearly with sample numerosity, in accord with the Weber law of compressed analog magnitude representations including magnitude and distance effects (Figures 2C and 2D) (Nieder, 2016). This well-organized layout was significantly less pronounced in the higher-frequency beta band, suggesting that working memory content can be separated by rhythmic, frequency-specific activity of neuronal populations ("channels") in the fronto-parietal association cortex.

Frequency-Specific Directed Neuronal Communication

We reasoned that the prefrontal and parietal cortex might synchronize in the observed frequency bands, which could support content-specific long-range neuronal communication. First, we calculated the phase-locking value (PLV) between LFP traces on simultaneously recorded PFC and VIP channel pairs (n = 4,848) as a measure of coherent neuronal population activity (Liebe et al., 2012). Rhythmic fronto-parietal connectivity in the beta band peaked during presentation of the sample and distractor (Figure 3A). By contrast, it was strongest in the delta and theta band during the memory delays, i.e., in the range where the sample information was preferentially represented (compare to Figures 2A and 2B). This suggests that the low-frequency channel is involved in the exchange of task-relevant information within the fronto-parietal network. At these lower frequencies, fronto-parietal synchrony increased particularly early and strongly in the second memory delay in trials without a distractor and preceded the increase in connectivity in the beta band (Figure 3B).

Second, we determined the direction of functional connectivity between prefrontal and parietal cortex using the phase-slope index (PSI) (Johnson et al., 2017; Nolte et al., 2008). Positive indices, indicating predominant PFC-to-VIP information flow,

Task- and Memory-Content-Dependent Neuronal Communication

Is this frequency-specific directed connectivity a fixed, inherent network property regardless of task demands (Hillebrand et al., 2016)? Alternatively, if it contributes to maintaining and manipulating information in working memory, changes in memory content as the trial progresses should lead to frequency changes in fronto-parietal neuronal synchrony. To address this question, we compared the functional connectivity of PFC sample-selective neurons with parietal cortex in the first and second memory
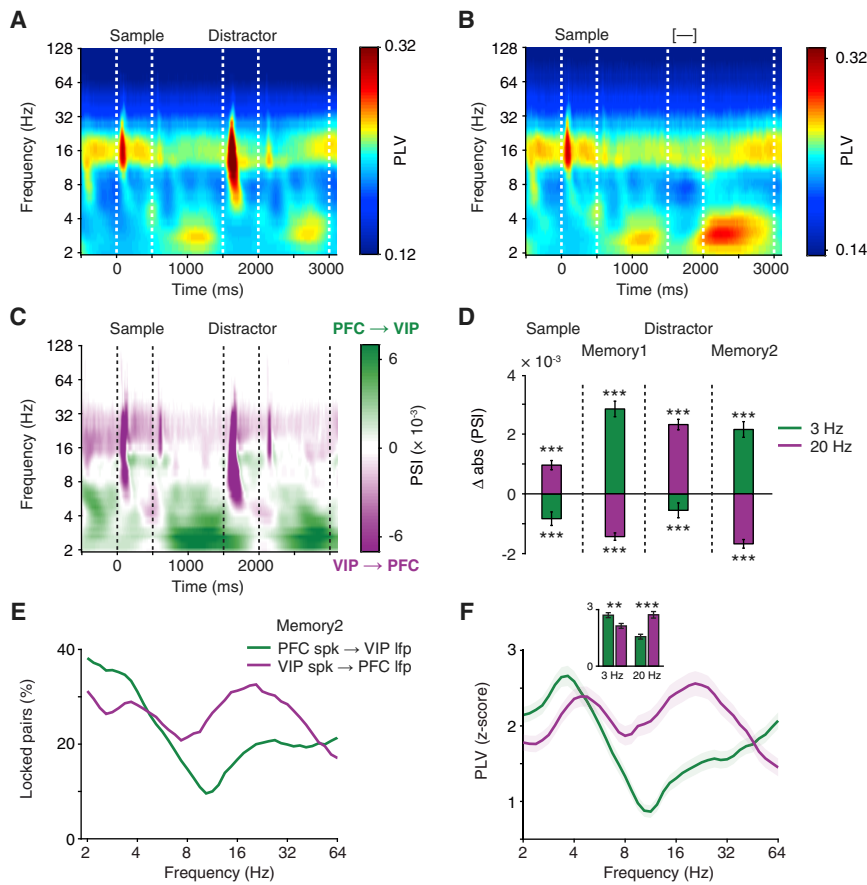
Frequency- and Phase-Specific Coding of Working Memory Content

So far, our results argue that beta-band connectivity in the fronto-parietal network is associated with memory traces of the most recent sensory input, while rhythmic activity in the delta and theta band could contribute to storing previously presented stimuli and separating distinct numerosities held in working memory. Oscillatory changes in excitability in a receiver neuronal population could serve as reading frames to decode multiplexed information about different individual stimuli nested within spike trains of sender neurons (Siegel et al., 2009). To explore such a potential coding mechanism, we investigated whether transmission of working memory content between the prefrontal and parietal cortex was frequency and phase dependent. We measured the amount of sample numerosity information carried by spikes of PFC sample-encoding neurons (ω^2 explained variance) at different parietal LFP phases (Siegel et al., 2009). In the first memory delay (n = 98 neurons), sample information was not distributed uniformly across all spikes but showed preferred, optimally encoding phases that differentiated between individual parietal LFP frequency bands, with a preference for faster rhythms in the beta and gamma range (Figures 5A and 5C). By contrast, sample information strongly shifted into the delta and theta range in the second memory delay (p = 0.03, permutation test; n = 73 neurons; Figures 5B and 5C). This frequency shift in phase-dependent coding from the first to the second memory delay closely resembled the task-dependent alternation between lower and higher frequencies in PFC-VIP spike-field locking (compare to Figure 4A).

The phase dependency of sample information in the delta and theta bands suggested that this frequency range might also

delays (n = 47 and n = 46, respectively; Figure 4A). Following sample presentation, when there was no competition for memory resources yet, spike-field phase locking (PLV) dominated in the beta band. However, it shifted to lower frequencies in the second memory delay after the distractor had been displayed (Figure 4A). Notably, in the second memory delay, PFC neurons carrying distractor information (n = 19) showed significantly stronger beta-band locking with area VIP than neurons carrying sample information (Figure 4B). A control analysis revealed that the described effects were independent of differences in LFP power, e.g., between the first and second memory delays, which might affect the robustness of spike-phase estimation (i.e., signal-to-noise ratio; Figure S5).

We next determined whether fronto-parietal connectivity also varied with working memory content (Salazar et al., 2012). We calculated a phase-locking selectivity index (PLSI) that captures variations in LFP-LFP PLV between the two regions as a function of varying sample and distractor numerosity (Figures 4C and 4D). In the second memory delay, sample-specific differences in synchrony were found exclusively in the delta and in particular the theta band, but not in the beta frequency range, where it was still present in the first memory delay (Figure 4C). This finding was reminiscent of our results obtained with the classifier operating on LFP power (Figure 2A). In contrast, distractor-specific synchrony differences were found only during presentation of the distractor and, here, most prominently in the beta band (Figure 4D).
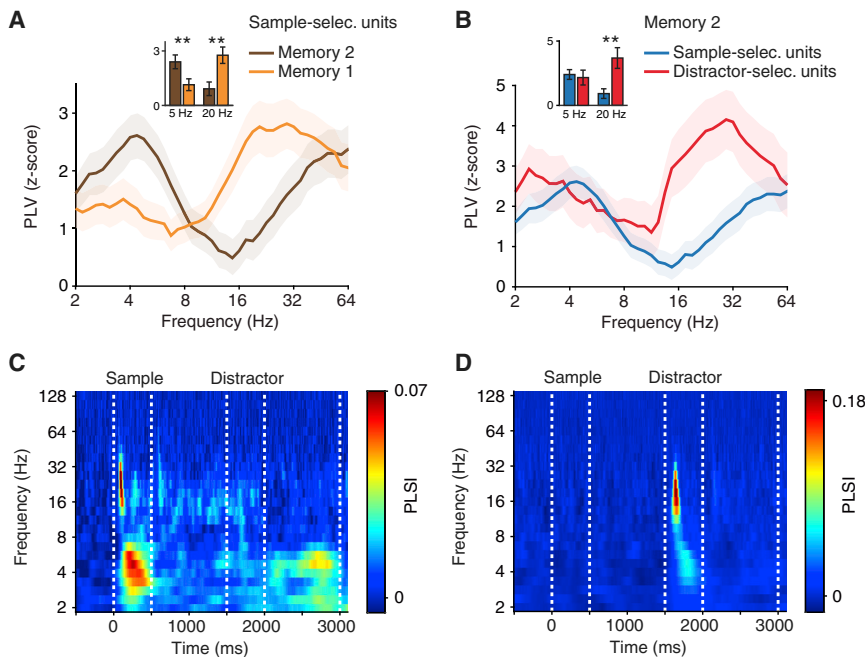
Figure 4. Task- and Memory-Content Dependence of Fronto-parietal Synchrony

(A) PLV between spikes of PFC sample-selective units and parietal LFPs recorded at sites with sample-selective units in the first and second memory delay (n = 47 and n = 46 PFC neurons, respectively; Z score from shuffled null distribution). Inset: mean PLV for both memory delays in the theta (5 Hz) and beta range (20 Hz).

(B) Same analysis as in (A) for PFC distractor-selective single units and parietal LFPs recorded at sites with distractor-selective units in the second memory delay (n = 19; n = 46 PFC sample-selective units (A) for comparison). Error bands and bars indicate SEM across neurons. **p < 0.01 (Wilcoxon rank sum test).

(C) Phase-locking selectivity index (PLSI) quantifying the degree to which fronto-parietal synchrony (LFP-LFP PLV) varied with sample numerosity.

(D) Same analysis as in (C) for the distractor numerosity. See also Figure S5.

accommodate the distractor numerosity without causing relevant interference. Indeed, encoding of the distractor numerosity was equally phase dependent (n = 73 distractor-selective neurons; Figures 5D and 5E). Notably, the optimally encoding theta phases for the sample and distractor numerosity were well separated and close to orthogonal (sample: −134° ± 24°, distractor: −26° ± 25°, p = 0.03, permutation test; Figure 5F). This means that, by reading out PFC spikes at optimal theta phases, a recipient population of VIP neurons could adjust and maximize the amount of transmitted sample or distractor information independently and without affecting coding of the other stimulus. These results were independent of whether the evoked responses were subtracted from the LFP during pre-processing or not (Figure S6; sample: −126° ± 27°, distractor: −32° ± 22°, p = 0.03, permutation test).

Local representation of the sample and distractor numerosity within PFC showed the same significant separation in theta phase (sample: 34° ± 20°, distractor: 134° ± 31°, p = 0.03, permutation test; Figure S7). In contrast to the phase coding between regions, however, local prefrontal distractor information was also phase dependent in the beta range (Figures S7B and S7C; sample: 151° ± 66°, distractor: 130° ± 52°, p = 0.64, permutation test; Figure S7E), further supporting a specialization of the beta and delta/theta working memory channels in function and content. The average phase difference between prefrontal and parietal LFPs in the theta band (180°, Figure S8A; a consequence of our common-average referencing [Shirhatti et al., 2016]) matched the difference in optimally encoding phases in this frequency range between local and cross-regional representations. To exclude that fronto-parietal phase-dependent coding merely reflected local phase dependency in PFC and the synchrony between the two regions, we performed a mediation analysis quantifying the influence of PFC LFPs on the synchrony between PFC spikes and VIP LFPs (Figure S8B). The strongest contributions of PFC LFPs were detected in the delta band in the memory delays. Importantly, however, the mediated proportion was 25% at maximum across all time and frequency bins, indicating that the large majority of PFC spike to VIP LFP synchrony was independent of PFC LFPs.

Behavioral Relevance of Frequency- and Phase-Specific Information Coding

If frequency-specific neuronal synchrony and information transmission play a role in working memory coding, they should be correlated with the animals' performance. To investigate the behavioral relevance of our findings, we first compared fronto-parietal LFP-LFP phase locking (PLV) in correct trials with short and long reaction times (first quartile versus fourth quartile; Figures 6A and 6B). Increased synchrony in the theta frequency band in the second memory delay resulted in shorter reaction times (1.0 ± 0.001 versus 0.976 ± 0.001, p < 10^{-4}, Wilcoxon rank sum test, Figure 6B). Neither delta nor beta connectivity were predictive of the animals' reaction times. We next examined phase-dependent coding of sample and distractor numerosities in the second memory delay of error trials. To ensure equal statistical power, we compared our results using correctly performed trials (Figure 5) with the results obtained after replacing randomly chosen correct trials with error trials (37% of trials replaced on average). For the sample numerosity, this selectively and substantially degraded phase-dependent coding in the theta frequency band (Figures 6C and 6E). By contrast, increased sample coding in the beta range negatively affected the animals' behavioral performance. A similar result was obtained for distractor coding (Figures 6D and 6F). A loss of phase-dependent coding in the upper theta/alpha band predicted forthcoming errors, whereas the opposite effect was present in the beta frequency band. While the theta channel promoted correct responses, prominent phase-dependent coding in the delta band tended to negatively affect the animals' performance (Figures 6E and 6F), demonstrating a clear functional
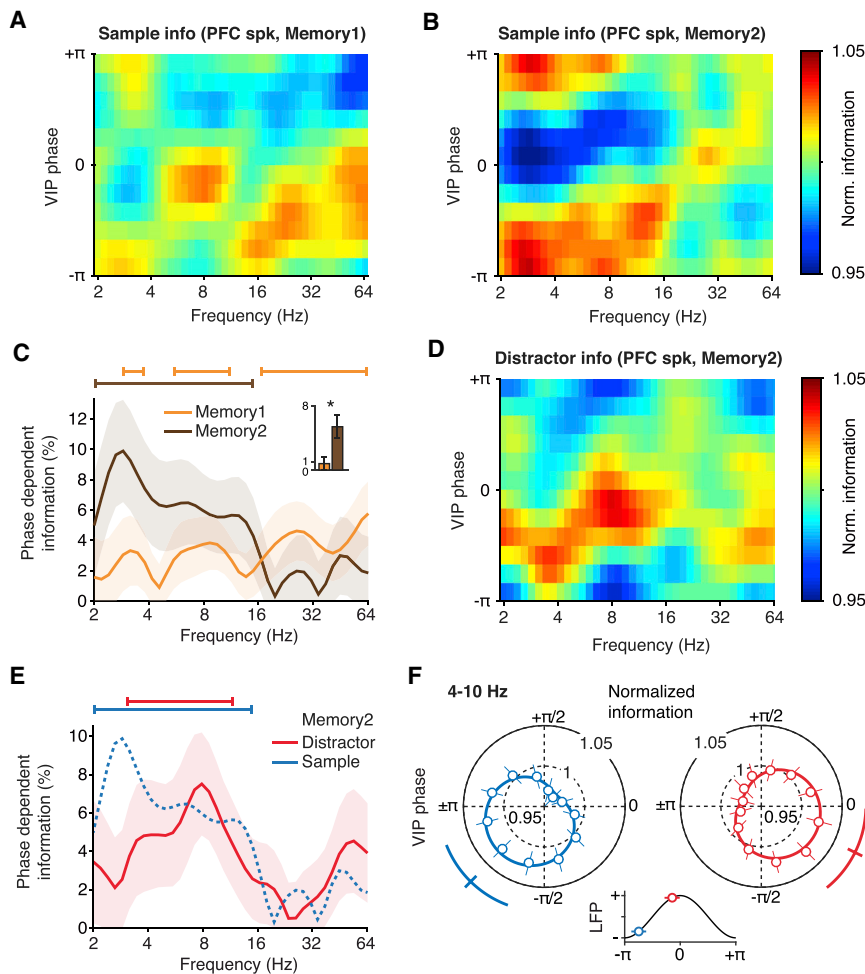
Figure 5. Frequency- and Phase-Dependent Fronto-parietal Transmission of Working Memory Content

(A) Mean normalized information (ω^2 explained variance) about the sample numerosity in correct trials contained in spikes of PFC sample-selective neurons in the first memory delay (n = 98) as a function of parietal LFP frequency and phase (all parietal sites).

(B) Same analysis as in (A) for the second memory delay (n = 73).

(C) Phase-dependent sample information carried by spikes of PFC sample-selective neurons in both memory delays as a function of parietal LFP frequency. Error bands indicate bootstrap SEMs. Bars indicate significant phase dependence (p < 0.01, permutation test). Inset: mean ratio of phase-dependency in the theta (4–10 Hz) versus beta range (12–32 Hz) with bootstrap SEMs. *p < 0.05, permutation test.

(D) Mean normalized information about the distractor numerosity in correct trials contained in spikes of distractor-selective PFC neurons in the second memory delay (n = 73) as a function of parietal LFP frequency and phase.

(E) Phase-dependent information carried by spikes of PFC sample- and distractor-selective neurons in the second memory delay as a function of parietal LFP frequency. Error bands and significance bars as in (C).

(F) Normalized information about the sample and distractor numerosity carried by PFC neurons during the second memory delay (B and D) as a function of the theta parietal LFP phase. Circles and bars indicate the normalized information for 12 phase bins and bootstrap SEMs. Solid traces indicate a cosine fit, the mean optimally encoding phase, and its bootstrap SEM. Inset: optimally encoding phases and SEMs on a schematic LFP oscillation (standard cosine). See also Figures S6–S8.

segregation in the low-frequency range with a sharp demarcation at 4 Hz.

DISCUSSION

We found that oscillatory population activity (LFPs) in the prefrontal and parietal cortex can represent working memory content in distinct frequency channels that shift with task demands. Working memory performance critically depended on prefrontal-to-parietal signaling in the theta band. A phase-dependent code in this frequency range differentiated between multiple memorized numerosities, which could allow selective indexing, readout, and long-range transmission of stored contents nested ("multiplexed") in spiking activity of single PFC neurons.

Previous analyses of behavioral and single-unit data acquired in the present task had shown that the distractor was not suppressed but instead represented together with the sample stimulus (Jacob and Nieder, 2014). We now observed a functional specialization of fronto-parietal neuronal rhythms in coding and separating working memory content. Information in the beta frequency range was sensory driven and reflected memory traces

of the most recently presented numerosity, irrespective of its behavioral relevance (sample or distractor; Figure 2, Figure S2, Figure S7B). Recent experiments have demonstrated dominant synchrony between parietal and prefrontal cortex in the beta band in working memory tasks with one to-be-memorized item and no competition for storage capacity by interfering distractors (Antzoulatos and Miller, 2016; Salazar et al., 2012). Our results extend these findings and suggest that parietal-to-prefrontal beta connectivity forms a channel for serial information transmission that is occupied by a single stimulus at a given time.

Theta oscillations are thought to be involved in the coding of sequentially presented items (Roux and Uhlhaas, 2014; Schroeder and Lakatos, 2009). In working memory tasks with multiple stimuli, theta activity is pronounced (Roux and Uhlhaas, 2014). Disrupting PFC function with theta-burst transcranial magnetic stimulation in human subjects reduces working memory performance and degrades memorized information stored in extrastriate visual cortex (Feredoes et al., 2011; Lee and D'Esposito, 2012). Enhancing theta-band activity and synchrony in the fronto-parietal network (Albouy et al., 2017; Hoy et al., 2016; Violante et al., 2017), in turn, improves subjects' performance in
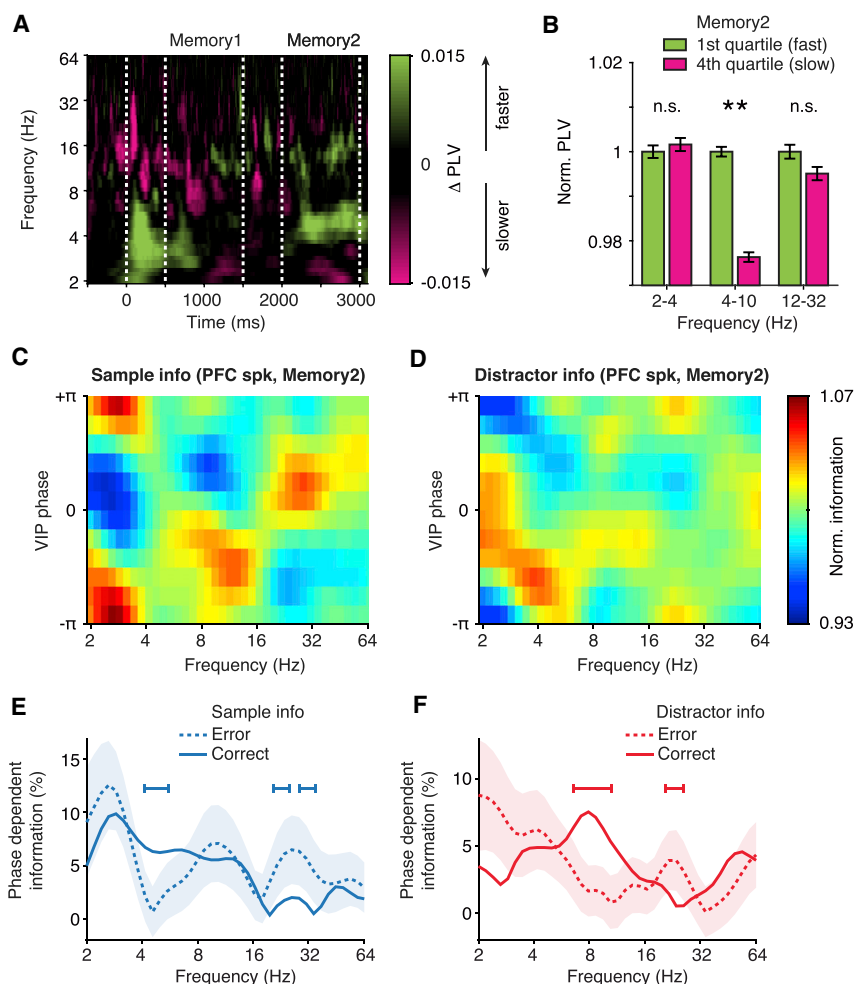
Figure 6. Behavioral Relevance of Frequency-Specific Memory Coding

(A) Difference in fronto-parietal LFP-LFP PLV between correct trials with the shortest and longest reaction times (first quartile and fourth quartile, respectively; n = 4,848 pairs).

(B) Mean fronto-parietal PLV in the second memory delay for the fastest and slowest trials in the delta (2–4 Hz), theta (4–10 Hz), and beta (12–32 Hz) frequency bands. Data are expressed as the mean across pairs, normalized for each frequency band to the PLV of the fastest trials. Error bars indicate SEM across pairs. **p < 0.01; n.s., not significant (Wilcoxon rank sum test).

(C) Mean normalized information about the sample numerosity contained in spikes of PFC sample-selective neurons in the second memory delay (n = 73) as a function of parietal LFP frequency and phase. Random subsets of correct trials were replaced with error trials.

(D) Same analysis as in (C) for distractor information in PFC distractor-selective neurons (n = 73).

(E) Comparison of phase-dependent sample information in PFC sample-selective neurons in the second memory delay between correct trials (Figure 5B) and after replacing correct trials with error trials (C). Error band indicates bootstrap SEM. Bars indicate significant differences (p < 0.05, permutation test).

(F) Same analysis as in (E) for phase-dependent distractor information in PFC distractor-selective neurons (comparison between D and Figure 5D).

working memory tasks. Our results now provide a mechanistic basis for these findings by showing that the prefrontal-to-parietal theta channel carries multiplexed information about individual memorized stimuli that is necessary to solve the task (Figures 2, 5, and 6). Changes in parietal excitability that are temporally aligned to prefrontal spiking activity could allow this "receiver" region to tune in to and read out distinct groups of PFC spikes, thereby disentangling the mixed selectivity of the "sender" neurons (communication through coherence [Fries, 2015]).

Notably, and in contrast to the sample, the amount of phase-dependent information about the distractor stimulus peaked in the upper theta or alpha frequency range. Distractor information in this band critically determined the animals' ability to solve the task (Figures 5D and 6F). Alpha activity has previously been associated with protecting working memory content from anticipated distracting events (Bonnefond and Jensen, 2012; Roux and Uhlhaas, 2014; Sauseng et al., 2009). Our data now suggest that inhibition of task-irrelevant information occurs by broadcasting a specific "blocking signal" in the alpha channel in form of the identity of the to-be-ignored stimulus.

In the delta range, information about the sample numerosity was strong, but not predictive, of the animals' performance (Figures 2, 5, and 6). Unlike in the theta band, we found a lack of

response acceleration by fronto-parietal connectivity in the delta range (Figure 6B) and a trend to increased numerosity information in error trials (Figures 6E and 6F). Without subtraction of evoked responses, the preferred encoding phases for the sample and distractor even coincided (Figure S6). Little is known about the role of delta oscillations in higher cognition. Multiple EEG studies have reported in particular frontal delta activity in a variety of behavioral tasks, including working memory (Harmony, 2013). It has been hypothesized that suppression of sensory inputs to and motor outputs from the frontal cortex could be associated with delta oscillations in the sense of a "functional de-afferentiation" of this brain region (Harmony, 2013). While more work is needed to explore these concepts, our results are in line with a role of fronto-parietal delta rhythms in general inhibitory control.

Parallel coding of information with mixed, but clearly separable, neuronal representations constitutes an attractive mechanism for rendering stored information resistant to interference, one of the hallmarks of working memory (Baddeley, 2012). Recent studies have shown that protection from distractors does not require PFC neurons to suppress or filter distracting information (Jacob and Nieder, 2014; Jacob et al., 2016). The present findings argue that this could be achieved instead by maintaining nested neuronal representations of memory content that are well separated and decodable by theta-frequency phase. If multiple stimuli are encoded across the oscillatory

cycle, a phase-dependent coding scheme could also contribute to the capacity limits of working memory (Buschman et al., 2011; Jensen and Lisman, 1998; Lisman and Idiart, 1995; Siegel et al., 2009): phase space per cycle is finite, and increasing overlap between adjacent stimuli would eventually curb the ability to resolve the stored information during retrieval.

Phase-dependent coding of the sample and distractor was also present locally in PFC (Figure S7), in accordance with a previous study where monkeys were required to explicitly memorize two sequentially presented items (Siegel et al., 2009). However, in contrast to this report, we did not observe a significant difference in beta-phase encoding in PFC, but instead a strong effect in the theta frequency band. This suggests that the mechanisms of prefrontal information storage are flexible and can adapt to specific task demands (Figure 4, Figure S5). Local prefrontal oscillatory activity during working memory has also recently been shown to occur mainly in brief, discrete bursts, not as sustained, long-lasting bands (Lundqvist et al., 2016, 2018). More experiments with a focus on single-trial analyses are needed to determine the exact temporal dynamics of the phase dependency described here.

Frequency-specific synchrony is a wide-spread neuronal phenomenon and has been reported in various cognitive tasks (Buschman and Miller, 2007; Phillips et al., 2014; Place et al., 2016) and in different brain networks involving for example sensory cortices (Gregoriou et al., 2009; Liebe et al., 2012; Michalareas et al., 2016) and the hippocampus (Place et al., 2016). An increasing body of evidence is showing that different frequencies play specialized roles in cortico-cortical communication. For example, in the primate visual system, feedforward (bottom-up) influences are conveyed predominately by gamma-band synchrony, whereas the alpha/beta band is associated with feedback (top-down) signaling (Bastos et al., 2015; Michalareas et al., 2016; van Kerkoerle et al., 2014). While our results are consistent with the concept that higher and lower frequencies underlie feedforward (parieto-frontal) and feedback (fronto-parietal) synchrony, respectively, the cross-regional interactions we observed here were shifted down in frequency to the beta and theta range (Johnson et al., 2017). One possibility for this difference is that our recordings were performed in a pair of higher-order association areas that are crucial for cognitive control and not primarily involved in relaying sensory information (Phillips et al., 2014). Future work must therefore reveal whether the frequency- and phase-dependent structuring of working memory content we describe here constitutes a general organizing principle in long-range routing of information.

STAR★METHODS

Detailed methods are provided in the online version of this paper and include the following:

- KEY RESOURCES TABLE
- CONTACT FOR REAGENT AND RESOURCE SHARING
- EXPERIMENTAL MODEL AND SUBJEC DETAILS
- METHOD DETAILS
  ○ Surgical procedures
  ○ Task and stimuli

  ○ Electrophysiology
- QUANTIFICATION AND STATISTICAL ANALYSIS
  ○ Preprocessing
  ○ Spectral transformation
  ○ Power
  ○ Phase
  ○ Cross-spectrum
  ○ Phase-locking value
  ○ Phase Locking Selectivity Index
  ○ Phase-slope index
  ○ Wiener-Granger causality
  ○ Naive Bayes decoding
  ○ Phase-dependent information
  ○ Complex mediation
- DATA AND SOFTWARE AVAILABILITY

AUTHOR CONTRIBUTIONS

S.N.J. designed and performed experiments, analyzed data, and wrote the paper; D.H. analyzed data and wrote the paper; A.N. designed experiments and wrote the paper.

DECLARATION OF INTERESTS

The authors declare no competing interests.

REFERENCES

Albouy, P., Weiss, A., Baillet, S., and Zatorre, R.J. (2017). Selective Entrainment of Theta Oscillations in the Dorsal Stream Causally Enhances Auditory Working Memory Performance. Neuron 94, 193–206.e5.

Antzoulatos, E.G., and Miller, E.K. (2016). Synchronous beta rhythms of frontoparietal networks support only behaviorally relevant representations. eLife 5, 568.

Baddeley, A. (2012). Working memory: theories, models, and controversies. Annu. Rev. Psychol. 63, 1–29.

Bastos, A.M., Vezoli, J., Bosman, C.A., Schoffelen, J.-M., Oostenveld, R., Dowdall, J.R., De Weerd, P., Kennedy, H., and Fries, P. (2015). Visual areas exert feedforward and feedback influences through distinct frequency channels. Neuron 85, 390–401.

Berens, P. (2009). CircStat: A MATLAB toolbox for circular statistics. J. Stat. Softw. 31, 1–21.

Boca, S.M., Sinha, R., Cross, A.J., Moore, S.C., and Sampson, J.N. (2014). Testing multiple biological mediators simultaneously. Bioinformatics 30, 214–220.

Bonnefond, M., and Jensen, O. (2012). Alpha oscillations serve to protect working memory maintenance against anticipated distracters. Curr. Biol. *22*, 1969–1974.

Buschman, T.J., and Miller, E.K. (2007). Top-down versus bottom-up control of attention in the prefrontal and posterior parietal cortices. Science *315*, 1860–1862.

Buschman, T.J., Siegel, M., Roy, J.E., and Miller, E.K. (2011). Neural substrates of cognitive capacity limitations. Proc. Natl. Acad. Sci. USA *108*, 11252–11255.

Buschman, T.J., Denovellis, E.L., Diogo, C., Bullock, D., and Miller, E.K. (2012). Synchronous oscillatory neural ensembles for rules in the prefrontal cortex. Neuron *76*, 838–846.

D'Esposito, M., and Postle, B.R. (2015). The cognitive neuroscience of working memory. Annu. Rev. Psychol. *66*, 115–142.

Dotson, N.M., Salazar, R.F., and Gray, C.M. (2014). Frontoparietal correlation dynamics reveal interplay between integration and segregation during visual working memory. J. Neurosci. *34*, 13600–13613.

Feredoes, E., Heinen, K., Weiskopf, N., Ruff, C., and Driver, J. (2011). Causal evidence for frontal involvement in memory target maintenance by posterior brain areas during distracter interference of visual working memory. Proc. Natl. Acad. Sci. USA *108*, 17510–17515.

Fries, P. (2015). Rhythms for Cognition: Communication through Coherence. Neuron *88*, 220–235.

Fusi, S., Miller, E.K., and Rigotti, M. (2016). Why neurons mix: high dimensionality for higher cognition. Curr. Opin. Neurobiol. *37*, 66–74.

Granger, C. (1969). Investigating causal relations by econometric models and cross-spectral methods. Econometrica *37*, 424–438.

Gregoriou, G.G., Gotts, S.J., Zhou, H., and Desimone, R. (2009). High-frequency, long-range coupling between prefrontal and visual cortex during attention. Science *324*, 1207–1210.

Gupta, N., Singh, S.S., and Stopfer, M. (2016). Oscillatory integration windows in neurons. Nat. Commun. *7*, 13808.

Harmony, T. (2013). The functional significance of delta oscillations in cognitive processing. Front. Integr. Neurosci. *7*, 83.

Hillebrand, A., Tewarie, P., van Dellen, E., Yu, M., Carbo, E.W.S., Douw, L., Gouw, A.A., van Straaten, E.C.W., and Stam, C.J. (2016). Direction of information flow in large-scale resting-state networks is frequency-dependent. Proc. Natl. Acad. Sci. USA *113*, 3867–3872.

Hoy, K.E., Bailey, N., Michael, M., Fitzgibbon, B., Rogasch, N.C., Saeki, T., and Fitzgerald, P.B. (2016). Enhancement of working memory and task-related oscillatory activity following intermittent theta burst stimulation in healthy controls. Cereb. Cortex *26*, 4563–4573.

Jacob, S.N., and Nieder, A. (2014). Complementary roles for primate frontal and parietal cortex in guarding working memory from distractor stimuli. Neuron *83*, 226–237.

Jacob, S.N., Stalter, M., and Nieder, A. (2016). Cell-type-specific modulation of targets and distractors by dopamine D1 receptors in primate prefrontal cortex. Nat. Commun. *7*, 13218.

Jensen, O., and Lisman, J.E. (1998). An oscillatory short-term memory buffer model can account for data on the Sternberg task. J. Neurosci. *18*, 10688–10699.

Jensen, O., and Tesche, C.D. (2002). Frontal theta activity in humans increases with memory load in a working memory task. Eur. J. Neurosci. *15*, 1395–1399.

Johnson, E.L., Dewar, C.D., Solbakk, A.-K., Endestad, T., Meling, T.R., and Knight, R.T. (2017). Bidirectional frontoparietal oscillatory systems support working memory. Curr. Biol. *27*, 1829–1835.e4.

Kornblith, S., Buschman, T.J., and Miller, E.K. (2016). Stimulus load and oscillatory activity in higher cortex. Cereb. Cortex *26*, 3772–3784.

Lee, T.G., and D'Esposito, M. (2012). The dynamic nature of top-down signals originating from prefrontal cortex: a combined fMRI-TMS study. J. Neurosci. *32*, 15458–15466.

Lewis, C.M., Bosman, C.A., Brunet, N.M., Lima, B., Roberts, M.J., Womelsdorf, T., de Weerd, P., Neuenschwander, S., Singer, W., and Fries, P. (2016). Two frequency bands contain the most stimulus-related information in visual cortex. bioRxiv. https://doi.org/10.1101/049718.

Liebe, S., Hoerzer, G.M., Logothetis, N.K., and Rainer, G. (2012). Theta coupling between V4 and prefrontal cortex predicts visual short-term memory performance. Nat. Neurosci. *15*, 456–462, S1–S2.

Lisman, J.E., and Idiart, M.A. (1995). Storage of 7 +/- 2 short-term memories in oscillatory subcycles. Science *267*, 1512–1515.

Lundqvist, M., Rose, J., Herman, P., Brincat, S.L., Buschman, T.J., and Miller, E.K. (2016). Gamma and Beta Bursts Underlie Working Memory. Neuron *90*, 152–164.

Lundqvist, M., Herman, P., Warden, M.R., Brincat, S.L., and Miller, E.K. (2018). Gamma and beta bursts during working memory readout suggest roles in its volitional control. Nat. Commun. *9*, 394.

MacKinnon, D.P., Fairchild, A.J., and Fritz, M.S. (2007). Mediation analysis. Annu. Rev. Psychol. *58*, 593–614.

Mendoza-Halliday, D., Torres, S., and Martinez-Trujillo, J.C. (2014). Sharp emergence of feature-selective sustained activity along the dorsal visual pathway. Nat. Neurosci. *17*, 1255–1262.

Merten, K., and Nieder, A. (2009). Compressed scaling of abstract numerosity representations in adult humans and monkeys. J. Cogn. Neurosci. *21*, 333–346.

Michalareas, G., Vezoli, J., van Pelt, S., Schoffelen, J.-M., Kennedy, H., and Fries, P. (2016). Alpha-beta and gamma rhythms subserve feedback and feedforward influences among human visual cortical areas. Neuron *89*, 384–397.

Nieder, A. (2016). The neuronal code for number. Nat. Rev. Neurosci. *17*, 366–382.

Nieder, A., and Miller, E.K. (2004). Analog numerical representations in rhesus monkeys: evidence for parallel processing. J. Cogn. Neurosci. *16*, 889–901.

Nieder, A., Freedman, D.J., and Miller, E.K. (2002). Representation of the quantity of visual items in the primate prefrontal cortex. Science *297*, 1708–1711.

Nieder, A., Diester, I., and Tudusciuc, O. (2006). Temporal and spatial enumeration processes in the primate parietal cortex. Science *313*, 1431–1435.

Nolte, G., Ziehe, A., Nikulin, V.V., Schlögl, A., Krämer, N., Brismar, T., and Müller, K.-R. (2008). Robustly estimating the flow direction of information in complex physical systems. Phys. Rev. Lett. *100*, 234101.

Oostenveld, R., Fries, P., Maris, E., and Schoffelen, J.-M. (2011). FieldTrip: Open source software for advanced analysis of MEG, EEG, and invasive electrophysiological data. Comput. Intell. Neurosci. *2011*, 156869.

Parthasarathy, A., Herikstad, R., Bong, J.H., Medina, F.S., Libedinsky, C., and Yen, S.-C. (2017). Mixed selectivity morphs population codes in prefrontal cortex. Nat. Neurosci. *20*, 1770–1779.

Pascual-Marqui, R.D., Faber, P., Kinoshita, T., Kitaura, Y., Kochi, K., Milz, P., Nishida, K., and Yoshimura, M. (2016). The dual frequency RV-coupling coefficient: a novel measure for quantifying cross-frequency information transactions in the brain. arXiv, arXiv:1603.05343 https://arxiv.org/abs/1603.05343.

Pascual-Marqui, R.D., Faber, P., Ikeda, S., Ishii, R., Kinoshita, T., Kitaura, Y., Kochi, K., Milz, P., Nishida, K., and Yoshimura, M. (2017). The cross-frequency mediation mechanism of intracortical information transactions. bioRxiv. https://doi.org/10.1101/119362.

Pesaran, B., Pezaris, J.S., Sahani, M., Mitra, P.P., and Andersen, R.A. (2002). Temporal structure in neuronal activity during working memory in macaque parietal cortex. Nat. Neurosci. *5*, 805–811.

Pesaran, B., Nelson, M.J., and Andersen, R.A. (2008). Free choice activates a decision circuit between frontal and parietal cortex. Nature *453*, 406–409.

Phillips, J.M., Vinck, M., Everling, S., and Womelsdorf, T. (2014). A long-range fronto-parietal 5- to 10-Hz network predicts "top-down" controlled guidance in a task-switch paradigm. Cereb. Cortex *24*, 1996–2008.

Place, R., Farovik, A., Brockmann, M., and Eichenbaum, H. (2016). Bidirectional prefrontal-hippocampal interactions support context-guided memory. Nat. Neurosci. *19*, 992–994.

Raghavachari, S., Kahana, M.J., Rizzuto, D.S., Caplan, J.B., Kirschen, M.P., Bourgeois, B., Madsen, J.R., and Lisman, J.E. (2001). Gating of human theta oscillations by a working memory task. J. Neurosci. *21*, 3175–3183.

Ramirez-Cardenas, A., Moskaleva, M., and Nieder, A. (2016). Neuronal representation of numerosity zero in the primate parieto-frontal number network. Curr. Biol. *26*, 1285–1294.

Rigotti, M., Barak, O., Warden, M.R., Wang, X.-J., Daw, N.D., Miller, E.K., and Fusi, S. (2013). The importance of mixed selectivity in complex cognitive tasks. Nature *497*, 585–590.

Rose, N.S., LaRocque, J.J., Riggall, A.C., Gosseries, O., Starrett, M.J., Meyering, E.E., and Postle, B.R. (2016). Reactivation of latent working memories with transcranial magnetic stimulation. Science *354*, 1136–1139.

Roux, F., and Uhlhaas, P.J. (2014). Working memory and neural oscillations: α-γ versus θ-γ codes for distinct WM information? Trends Cogn. Sci. *18*, 16–25.

Salazar, R.F., Dotson, N.M., Bressler, S.L., and Gray, C.M. (2012). Content-specific fronto-parietal synchronization during visual working memory. Science *338*, 1097–1100.

Sauseng, P., Klimesch, W., Heise, K.F., Gruber, W.R., Holz, E., Karim, A.A., Glennon, M., Gerloff, C., Birbaumer, N., and Hummel, F.C. (2009). Brain oscillatory substrates of visual short-term memory capacity. Curr. Biol. *19*, 1846–1852.

Schroeder, C.E., and Lakatos, P. (2009). Low-frequency neuronal oscillations as instruments of sensory selection. Trends Neurosci. *32*, 9–18.

Shirhatti, V., Borthakur, A., and Ray, S. (2016). Effect of reference scheme on power and phase of the local field potential. Neural Comput. *28*, 882–913.

Siegel, M., Warden, M.R., and Miller, E.K. (2009). Phase-dependent neuronal coding of objects in short-term memory. Proc. Natl. Acad. Sci. USA *106*, 21341–21346.

van Kerkoerle, T., Self, M.W., Dagnino, B., Gariel-Mathis, M.-A., Poort, J., van der Togt, C., and Roelfsema, P.R. (2014). Alpha and gamma oscillations characterize feedback and feedforward processing in monkey visual cortex. Proc. Natl. Acad. Sci. USA *111*, 14332–14341.

Violante, I.R., Li, L.M., Carmichael, D.W., Lorenz, R., Leech, R., Hampshire, A., Rothwell, J.C., and Sharp, D.J. (2017). Externally induced frontoparietal synchronization modulates network dynamics and enhances working memory performance. eLife *6*, 111.

Warden, M.R., and Miller, E.K. (2007). The representation of multiple objects in prefrontal neuronal delay activity. Cereb. Cortex *17* (*Suppl 1*), i41–i50.

Womelsdorf, T., Schoffelen, J.-M., Oostenveld, R., Singer, W., Desimone, R., Engel, A.K., and Fries, P. (2007). Modulation of neuronal interactions through neuronal synchronization. Science *316*, 1609–1612.

STAR★METHODS

KEY RESOURCES TABLE

REAGENT or RESOURCE	SOURCE	IDENTIFIER
Experimental Models: Organisms/Strains		
Monkey: *macaca mulatta*	German Primate Center	N/A
Software and Algorithms		
MATLAB	MathWorks	RRID: SCR_001622
FieldTrip toolbox	FieldTrip website	N/A
CircStat toolbox	MathWorks File Exchange	N/A

CONTACT FOR REAGENT AND RESOURCE SHARING

Further information and requests for resources and reagents should be directed to and will be fulfilled by the Lead Contact, Simon Jacob (simon.jacob@tum.de).

EXPERIMENTAL MODEL AND SUBJEC DETAILS

Two adult male rhesus monkeys (*Macaca mulatta*, monkey R and monkey W, 12 and 13 years old) were used in this study. All experimental procedures were in accordance with the guidelines for animal experimentation approved by the national authority, the Regierungspräsidium Tübingen.

METHOD DETAILS

Surgical procedures
Monkeys were implanted with two right-hemispheric recording chambers centered over the principal sulcus of the lateral prefrontal cortex (PFC) and the ventral intraparietal area (VIP) in the fundus of the intraparietal sulcus.

Task and stimuli
A detailed description of the monkeys' task and behavioral performance is provided elsewhere (Jacob and Nieder, 2014). The animals grabbed a bar to initiate a trial and maintained eye fixation (ISCAN, Woburn, MA) within 1.75° of visual angle of a central white dot. Stimuli were presented on a centrally placed gray circular background subtending 5.4° of visual angle. Following a 500 ms pre-sample (pure fixation) period, a 500 ms sample stimulus containing 1 to 4 dots was shown. The monkeys had to memorize the sample numerosity for 2,500 ms and compare it to the number of dots (1 to 4) presented in a 1,000 ms test stimulus. Test stimuli were marked by a red ring surrounding the background circle. If the numerosities matched (50% of trials), the animals released the bar (correct Match trial). If the numerosities were different (50% of trials), the animals continued to hold the bar until the matching number was presented in the subsequent image (correct Non-match trial). Match and non-match trials were pseudo-randomly intermixed. Correct trials were rewarded with a drop of water. In 80% of trials, a 500 ms interfering numerosity of equal numerical range was presented between the sample and test stimulus. The interfering numerosity was not systematically related to either the sample or test numerosity and therefore not useful for solving the task. In 20% of trials, a 500 ms gray background circle without dots was presented instead of an interfering stimulus, i.e., trial length remained constant (control condition, blank). Trials with and without interfering numerosities were pseudo-randomly intermixed. Stimulus presentation was balanced: a given sample was followed by all interfering numerosities with equal frequency, and vice versa. Throughout the monkeys' training on the distractor task, there was never a condition where a stimulus appearing at the time of the distractor was task-relevant.

Low-level, non-numerical visual features could not systematically influence task performance (Jacob and Nieder, 2014; Nieder et al., 2002): in half of the trials, dot diameters were selected at random. In the other half, dot density and total occupied area were equated across stimuli. CORTEX software (NIMH, Bethesda, MD) was used for experimental control and behavioral data acquisition. New stimuli were generated before each recording session to ensure that the animals did not memorize stimulus sequences.

Electrophysiology
Up to eight 1 MΩ glass-insulated tungsten electrodes (Alpha Omega, Israel) per chamber and session were acutely inserted through an intact dura with 1 mm spacing. To access VIP, electrodes were passed along the course of the intraparietal sulcus to a depth of 9 to 13 mm below the cortical surface (Jacob and Nieder, 2014; Nieder et al., 2006; Ramirez-Cardenas et al., 2016). Correct positioning

of the electrodes in VIP was verified by physiological criteria (responses to moving visual stimuli and tactile stimulation). We recorded from a total of 616 PFC sites (monkey R: 368, monkey W: 248) and 614 VIP sites (monkey R: 376, monkey W: 238). Extracellular neuronal signals were acquired with a unity-gain headstage and hardware bandpass-filtered into spiking activity (100 Hz – 8 kHz, sampling rate 40 kHz) and local field potentials (LFPs; 0.7 Hz – 170 Hz, sampling rate 1 kHz). Single units were recorded at random; no attempt was made to preselect for particular response properties. Signal amplification, filtering, and digitalization were accomplished with the MAP system (Plexon, Dallas, TX). Waveform separation was performed offline (Plexon Offline Sorter).

QUANTIFICATION AND STATISTICAL ANALYSIS

Data analysis was performed with MATLAB (MathWorks, Natick, MA) using custom scripts, the FieldTrip toolbox (Oostenveld et al., 2011) and the CircStat toolbox (Berens, 2009). To account for neuronal response latencies in prefrontal and parietal cortex (Jacob and Nieder, 2014), the starting and end points of all trial epochs were offset by 100 ms for analysis.

Preprocessing
Single units were included in the analysis if the following criteria were met: (*a*) their average firing rate across trials was at least 1 spike/s; (*b*) they were recorded for at least 1 correct trial in all 20 conditions (4 sample numerosities x 5 interfering numerosities including the control [0] condition); (*c*) they modulated their firing rate in the course of the trial (one-way analysis of variance (ANOVA) with average firing rates in the pre-sample (fixation), sample, first memory, distractor, second memory epochs; evaluated at $p < 0.05$).

    LFP traces were mean-centered, filtered for line noise removal (4th order Butterworth notch at 50 Hz and first and second harmonics), and re-referenced to the average of all prefrontal and parietal electrodes within a session, unless stated otherwise. Signals phase-locked to stimulus presentation (i.e., event-related potentials, ERP) were removed by subtracting the average across trials from individual trials, unless stated otherwise. ERP subtraction was performed separately for all analyzed trial subsets.

Spectral transformation
Complex time-frequency representations X of single LFP trials or binary spike trains were estimated by convolution of signal x with complex kernels k:

$$X(t, \omega) = x(t) * k(t, \omega)$$

where t and ω are time and frequency, respectively, * is the convolution operator and k represents frequency-dependent Hanning-tapered complex sinusoids:

$$k(t, \omega) = A\left(1 - \cos\left(\frac{2\pi t\omega}{q}\right)\right)e^{2i\pi t\omega}$$

where A is a constant normalizing k to unit power and q is the kernel width in number of cycles. Except for the analysis of Wiener-Granger causality (see below), which required a linear frequency axis for algorithmic reasons, we used frequencies ranging from 2 to 128 Hz, logarithmically spaced in steps of $2^{1/8}$, and a kernel width of 3. For spike-LFP measures, complex Fourier coefficients were obtained from X at the individual spike times.

Power
The time-varying power pow_x of signal x at frequency ω was computed as the squared norm of its time-frequency transformation:

$$pow_x(t, \omega) = |X(t, \omega)|^2$$

Power was averaged across trials, sessions, and electrodes and z-scored to baseline (500 ms pre-sample epoch):

$$z_{pow_x}(t, \omega) = \frac{pow_x(t, \omega) - \mu_{BL}(\omega)}{s_{BL}(\omega)}$$

where $\mu_{BL}(\omega)$ and $s_{BL}(\omega)$ are the mean and standard deviation, respectively, of $pow_x(t, \omega)$ during baseline at frequency ω.

Phase
The time-varying phase φ_x of signal x at frequency ω is the argument of the complex Fourier coefficients X:

$$\varphi_x(t, \omega) = \arg(X(t, \omega))$$

Cross-spectrum
The complex time- and frequency dependent cross-spectrum crs_{xy} of signals x and y is the product of their conjugated spectral decompositions X and Y:

$$crs_{xy}(t, \omega) = X(t, \omega)Y(t, \omega)^*$$

where * is the complex conjugate.

Phase-locking value

The frequency-dependent phase-locking value *PLV* was computed as the norm of the average across observed phases:

$$PLV(\omega) = \left| \frac{1}{R} \sum_{r=1}^{R} e^{i\varphi(r,\omega)} \right|$$

where $\varphi(r,\omega)$ is the cross-electrode phase $\arg(crs_{xy}(\omega))$ at trial r and frequency ω (LFP-LFP PLV) or the spike phase of spike r at frequency ω (spike-LFP or spike-field PLV), and R is the number of observations (trials or spikes, respectively). Because the PLV is biased toward 1 for low sample sizes, we set the minimum number of observations to 50.

Spike-field PLVs for individual units were computed for all available unit-LFP pairs, averaged across pairs and then z-scored using the mean and standard deviation of a null distribution obtained by randomly shuffling the association of single-trial spike train and corresponding LFP trace within a session before spike phase estimation (n = 1,000) (Buschman et al., 2012). In an additional analysis to control for effects of varying LFP power on the robustness of spike phase estimation, spikes were stratified according to their associated LFP magnitude. At both 5 Hz and 20 Hz, we computed histograms of the spike-associated LFP magnitudes in the two conditions that were compared (e.g., first and second memory delay). This yielded a ratio of spike counts at every magnitude bin, which we used as probabilities for random subsampling of spikes. A spike was included in the PLV analysis if a sample drawn from a uniform distribution on [0,1] was less than or equal to the magnitude-associated probability.

For the PLV analysis in fast and slow trials, correct match trials were separated into quartiles based on reaction times (we did not include non-match trials because the second test image following the non-match was always a match and therefore predictable). Trial types (no distractor, repeat sample, true distractor) were matched across subsets, i.e., a given condition appeared equally often in the first and fourth quartile. ERPs were computed and subtracted separately for each subset.

Phase Locking Selectivity Index

To determine whether neuronal synchrony was stimulus-specific, we computed a PLV selectivity index (PLSI) based on an approach reported in (Salazar et al., 2012), exchanging coherence for PLV. PLSI is a mutual information measure and was computed as a function of time and frequency:

$$PLSI(t,f) = \sum_{r}\sum_{s} P(s)P(r \,|\, s)\log_2 \frac{P(r \,|\, s)}{P(r)}$$

with

$$P(r) = \sum_{s} P(r \,|\, s)P(s)$$

where $P(r)$, $P(s)$ and $P(r|s)$ are the probabilities of the response (i.e., PLVs), the stimulus (i.e., numerosities), and the conditional probability of the response given the stimulus (i.e., PLVs at individual numerosities), respectively. Since the PLV is an average measure across trials, we estimated $P(r|s)$ in increments of 0.01 on [0 1] using a normal distribution with mean $\mu = PLV_s$ and standard deviation σ estimated using a jackknife procedure:

$$\sigma = \sqrt{\frac{n-1}{n}\sum_{t=1}^{n}(x_t - \overline{x})^2}$$

with n being the number of trials for a given stimulus, x_t the jackknife PLV with trial t left out and x the mean across jackknife samples. For statistical assessment we computed a semi-generalized surrogate distribution of the $PLSI_{surr}$. At each of 1,000 iterations, condition labels were randomly shuffled across trials and PLSI was computed for one randomly chosen combination of channels. To mitigate underestimation of the bias of PLSI due to the use of a semi-generalized procedure, we corrected PLSI values by a factor α, which sets the average PLSI across frequency and time bins during the baseline to 0:

$$PLSI_{corr} = \alpha E_{PLSI}$$

with

$$\alpha = \frac{\sum_{t,f} PLSI}{\sum_{t,f} E_{PLSI}}$$

where t are the time bins during the baseline [-0.5 0]s, f are all frequency bins [2 128] and E_{PLSI} is the expected value from the surrogate distribution:

$$E_{PLSI} = \sum_{n} PLSI_{surr}(n)P(PLSI_{surr}(n))$$

evaluated at n = 500 bins.

Phase-slope index

The phase-slope index (PSI) is used to infer dominant unidirectional interactions, i.e., the net flow of information. It is based on the idea that the time lag required for a signal to travel from one location to another constitutes a frequency-dependent cross-regional phase difference which results in a phase-slope across frequencies (Nolte et al., 2008). The frequency-dependent PSI_{xy} of signals x and y was computed from the conjugated complex coherencies of neighboring frequencies:

$$PSI_{xy}(\omega_f) = \Im\left(\sum_{f}^{f+1} coh_{xy}^*(\omega_f)coh_{xy}(\omega_{f+1})\right)$$

where $\Im(\cdot)$ is the imaginary part, $coh_{xy}(\omega_f) = crs_{xy}/\sqrt{pow_x(\omega_f)pow_y(\omega_f)}$ the complex coherency and * the complex conjugate.

Wiener-Granger causality

Wiener-Granger causality (WGC) quantifies how the inclusion of past values of signal y improves the prediction of signal x in comparison to an autoregressive model of x (Granger, 1969). We calculated frequency-dependent $WGC_{x \to y}(\omega)$ from signal x to y at frequency ω as follows:

$$WGC_{x \to y}(\omega) = \ln\left(\frac{pow_y(\omega)}{pow_y(\omega) - \left(\Sigma_{xx} - \frac{\Sigma_{yx}^2}{\Sigma_{yy}}\right)\left|H_{yx}(\omega)\right|^2}\right)$$

where $pow_y(\omega)$ is the power of signal y at frequency ω, Σ_{xx} and Σ_{yy} noise variances of signal x and y, respectively, and Σ_{yx} the noise covariance of signals x and y in their auto-regressive models and $H_{yx}(\omega)$ is the spectral transfer matrix. We derived the noise covariance matrix Σ and $H_{yx}(\omega)$ by spectral factorisation of the trial-averaged cross-spectral density crs_{xy} using the Wilson-Burg algorithm as implemented in FieldTrip.

Naive Bayes decoding

The amount of information about the sample or distractor numerosity contained in local oscillatory activity was quantified using a Naive Bayes classifier (MATLAB Machine Learning Toolbox) (Lewis et al., 2016). For each time-frequency bin, a classifier was trained on the LFP power of 75% of randomly chosen trials. The feature vector comprised data from all prefrontal or parietal recording sites of an individual session. The remaining 25% of trials were used to test the classifier. We interpreted the numerosity with the highest posterior probability as the classifier's prediction for a given trial. Accuracy was calculated as the ratio of correctly predicted trials to all test trials. For decoding of the distractor numerosity, we excluded the control condition trials (i.e., no distractor presented). Accuracy was averaged across sessions.

Phase-dependent information

To quantify the phase-dependent information about the sample and distractor numerosity that was carried by a neuron's spiking activity, we grouped spikes by LFP phase into 12 equally spaced bins (Siegel et al., 2009). The information $I(\omega,b,s)$ of spikes at frequency ω and in phase bin b about stimulus s was computed using the explained variance measure:

$$I(\omega,b,s) = \frac{SS_{eff} - df_{eff}MS_{error}}{SS_{total} + MS_{error}}$$

where the individual terms are derived from a one-way ANOVA across trials: SS_{eff} is the sum of squares of the effect, df_{eff} the degrees of freedom, MS_{error} the mean squared error and SS_{total} the total sum of squares. $I(\omega,b,s)$ for individual units was computed for all available unit-LFP pairs, averaged across pairs and smoothed with a two-dimensional Hanning kernel (0.5 octave by 90° at FWHM). $I(\omega,b,s)$ was then averaged across units and normalized to the average information across phase bins per frequency:

$$I_{norm}(\omega,b,s) = \frac{\frac{1}{U}\sum_u^U I_u(\omega,b,s)}{\frac{1}{B}\sum_b^B \frac{1}{U}\sum_u^U I_u(\omega,b,s)}$$

where U is the number of units and B is the number of phase bins.

Phase-dependent information (PDI) was quantified by the peak-to-mean modulation of a cosine fit to the phase-binned information $I_u(\omega,b,s)$ on a per-unit basis (prior to normalization). The modulation is a measure of the non-uniformity of the magnitudes of the phase-binned information around an origin-centered circle in the complex plane (Siegel et al., 2009):

$$PDI(\omega,s) = 4\frac{\left|\sum_u^U\sum_b^B I_u(\omega,b,s)e^{i\lambda_b}\right|}{\sum_u^U\sum_b^B I_u(\omega,b,s)}$$

The SEM was estimated from bootstrapping across units (n = 1,000 iterations), i.e., the distribution of PDI values obtained from units subsampled with replacement from the entire pool of units used in the computation of the observed value (uniform probability

across units; 98 and 73 units for the first and second memory delay, respectively). PDI was tested for significance by shuffling the association of binned spikes and corresponding phases within frequencies of $I(\omega,b,s)$ before smoothing (n = 10,000). A given frequency was labeled as carrying significant PDI if the observed PDI exceeded 99% of values in the null distribution (p < 0.01, one-sided) and it was part of a 'cluster' of at least two consecutive significant frequency bins.

To investigate the relevance of phase-dependent information coding for the animals' working memory performance, we replaced a subset of correct trials with the available error trials before computing $I(\omega,b,s)$. This procedure ensures equal statistical power at the cost of underestimating the behavioral effects. Differences in PDI were tested for statistical significance using a null distribution of differences generated by shuffling outcome labels (correct versus error trial) of smoothed $I_u(\omega,b,s)$ (n = 1,000, p = 0.05, two-tailed).

The optimally encoding phase $\varphi_{opt}(\omega,s)$ was defined as the peak phase of a cosine fit to $I(\omega,b,s)$, i.e., the phase of the average vector across phases and units:

$$\varphi_{opt}(\omega, s) = \arg\left(\sum_{u}^{U} \sum_{b}^{B} I_u(\omega, b, s) e^{j\lambda_b} \right)$$

Phase and $I_{norm}(\omega,b,s)$ SEM were calculated after smoothing by bootstrapping across units (n = 10,000).

Complex mediation

We investigated the influence of prefrontal LFPs on the synchrony between prefrontal spikes and parietal LFPs using complex mediation analysis. This quantifies the contribution of an independent variable x on a dependent variable y taking into account the influence of a third, mediating variable z. For univariate real data, mediation can be described using regression coefficients c and c' of y regressed on x and x and z: $y = cx$ and $y = c'x + bz$ (MacKinnon et al., 2007). Here, c represents the overall effect of x on y, while c' represents the partial effect of x on y taking into account the partial effect of z on y. Thus, the fraction mediated is given by 1 - (c'/c). To render the mediation effect independent of the variance of the underlying data, (partial) correlation coefficients can be used (Boca et al., 2014). The fraction mediated becomes 1 - ($r_{xy|z}/r_{xy}$), with r_{xy} and $r_{xy|z}$ representing the correlation coefficient of x and y and the partial correlation coefficient of x and y conditional on z, respectively. Finally, generalizing this approach to complex valued multivariate data, we used the RV coefficient of Escoufier as proposed recently (Pascual-Marqui et al., 2016, 2017), which is equivalent to the squared correlation coefficient for univariate real data.

We computed the fraction mediated θ_m as

$$\theta_m = 1 - \sqrt{RV_{xy|z}/RV_{xy}}$$

with the RV coefficient

$$RV_{x,y} = \frac{tr\left(S_{x,y}S_{x,y}^*\right)}{\sqrt{tr\left(S_{x,x}^2\right)}\sqrt{tr\left(S_{y,y}^2\right)}}$$

and the partial RV coefficient

$$RV_{xy|z} = \frac{tr\left[\left(S_{zx} - S_{zy}S_{yy}^{-1}S_{yx}\right)\left(S_{zx} - S_{zy}S_{yy}^{-1}S_{yx}\right)^*\right]}{\sqrt{tr\left[\left(S_{zz} - S_{zy}S_{yy}^{-1}S_{yz}\right)^2\right]}\sqrt{tr\left[\left(S_{xx} - S_{xy}S_{yy}^{-1}S_{xz}\right)^2\right]}}$$

where S_{xy} is the variance-covariance matrix of matrices x and y, $tr(\cdot)$ is the trace of a matrix, and * denotes the complex conjugate. Here, the matrices x, y, and z are complex valued Fourier coefficients grouped as blocks of subcomponents, i.e., all prefrontal LFP channels, all parietal LFP channels and all prefrontal spike channels per session.

DATA AND SOFTWARE AVAILABILITY

Data and analysis software for this paper are available from the lead contact upon reasonable request.